

## Effect of Preform Geometry on the Material Behaviour and the Densification Mechanism during Hot Upset Forging of Sintered AISI 9840 P/M Steel Produced Using Elemental Powders

Manoj Kumar<sup>1</sup>, Dr. (Mrs.) Shashi Krishna Pandey<sup>2</sup>, Dr. (Mrs.) R.Nagalakshmi<sup>3</sup>,  
Dr. K.S. Pandey<sup>4</sup>

<sup>1</sup>Former, M. Tech. Student, Dept. of MME, National Institute of Technology, Tiruchirappalli-620015, TamilNadu, India,

<sup>2</sup>Director, National Institute of Technology, Puducherry, Karaikal 609 605;

<sup>3</sup>Manager, Welding Research Institute, Bharat Heavy Electricals Limited, Tiruchirappalli 620014, Tamil Nadu, India,

<sup>4</sup>Former Professor, Department of Metallurgical and Materials Engineering, National Institute of technology, Tiruchirappalli-620 015, Tamil Nadu, India.,

**Abstract:** The present investigation pertains to generate experimental data in order to establish the influence of initial preform geometries on the material behaviour and the operative densification mechanism/s during hot upset forging of sintered AISI 9840 P/M Steel composition prepared from the elemental powders. Powder blend corresponding to AISI 9840= C(0.4%), Mn(0.8%), Si(0.3%), Ni(1.0%), Cr(0.8%), Mo(0.25%) and Fe(96.4%) composition was prepared on a pot mill and the blending was carried out for a period<sup>1</sup> of 16hrs. while maintaining the powder to ball ratio 1.1: 1 by weight. Compacts of 27.5mm diameter and 12 - 24mm heights were prepared from the aforesaid blend in the density range of 84±1 percent of theoretical density by applying accurately controlled pressures in the range of 460±10 MPa and by taking pre-weighed powders. Indigenously developed ceramic coating was applied all over the compact surfaces and dried under an ambient conditions for a period of 10- 12 hrs. These ceramic coated compacts were recoated 90° to the previous coating and re- dried under the aforesaid conditions. These ceramic coated preforms were sintered in an electric muffle furnace for a period of 90 minutes at 11500±10°C. Immediately after the completion of the sintering schedule, the preforms corresponding to 0.45, 0.68 and 0.92 initial aspect ratios were axially hot forged to different height strains. Analysis of the experimental data has revealed that the lower aspect ratio preforms densified rapidly compared to higher aspect ratios and the densification curves corresponded to a third order polynomial of the form:  $(\rho_f/\rho_{th}) = a_0 + a_1 \epsilon_h + a_2 \epsilon_h^2 + a_3 \epsilon_h^3$ ; where,  $\epsilon_h = \ln (H_0/H_f)$  and  $a_0, a_1, a_2$  and  $a_3$  are empirically determined constants. Further analysis has established that the Poisson's ratio would always remain less than one half and will have the tendency to approach to a limiting value of 0.5 in the near vicinity of the theoretical density. Influence of the preform geometry is established to be quite pronounced and has affected the densification curves and Poisson's ratio with density.

**Key words:** Aspect ratio, ceramic coating, compacts, densification, hot forging.

### I. Introduction

Long before furnaces were developed that could approach the melting points of most of the metals, the, Powder Metallurgy (P/M) principles were invoked to consolidate powders to useful shapes. About 3000 BC, the Egyptians used "sponge iron" for making tools. In this early process, iron oxide was heated in a charcoal and crushed shell fire which was intensified by air blasts from bellows to reduce the oxide to a spongy metallic iron. The resulting hot sponge iron was then hammered to weld the particles together. However, the final shapes were obtained by simple forging procedures described elsewhere [1]. These crude forms of P/Multimately led to the development of one of the commercial methods for producing iron powder. Grinding the sponge iron to fine particles and heating these particles in hydrogen atmosphere removes the oxygen from the oxide and also softens the particles [2]. Commercial P/M now spans the density spectrum from highly porous metal filters to self-lubricating bearings and P/M parts with well controlled density to fully dense P/M wrought metal systems [3]. Manufacturing of precision engineering components from powder metallurgy route has on date become an established mass production technology and the major products of this route include the self-lubricating

bearings, filters, structural and electrical parts, electrical contacts, cemented carbide, diamond tools and frictional materials. Basically P/M is an art and science of producing fine metal powders and objects finished and semi-finished from individual, mixed or alloyed metal powders with or without the inclusions of non-metallic constituents [4 - 7]. The process has acquired more competitive status in comparison to the other metal forming technologies and powder metallurgy is growing continuously throughout the world. Powder preform forging (PPF) is a process in which sintered or un-sintered metal powders or preforms are hot formed in confined dies. Truly speaking, powder forging is a deformation processing technique aimed at enhancing the density of P/M parts, and, thus, their performance characteristics [4]. A major key factor in successful powder preform forging is the proper preform design. Preform design [8, 9] has a significant effect on metal flow and the distribution of stresses in the deforming preform. These factors, in turn, affect the densification and void fracture of the material. In general, sufficient metal flow must take place to achieve full density and good bonding [10]. However, increasing the amount of metal flow would increase the possibility of fracture. Thus, the preform shape must fall between fracture limits and the threshold for the best properties [11 - 13]. Preform design for each complex part must be taken in account on an individual basis. Nevertheless, some guidelines can always be obtained from the forging of a simple generic shape. An example, reported for flanged hub shape is described elsewhere [12]. Working of a conventional cast or wrought material invariably does not involve any change in the volume of the material. Basically this constancy of volume is one of the most striking factors used in the development of theory of plasticity and the metal working theories. In contrast to the constancy of volume that occurs in working of the conventional material, is the non-constancy of volume or a definite decrease in volume, which occurs in the deformation of P/M preforms [9, 14, 15]. The magnitude of the change in volume, i.e., likely to occur in deforming the P/M preforms depends upon the preform density and the amount of deformation. Nearly 30 to 40 % of the voids are present in the sintered preforms and, therefore, while deforming them, consideration must be made to the manner in which the voids deform during the compressive mode of loading. Thus, the material and the voids begin to flow under the influence of compressive loading and the deformation of voids continues to increase under the developed shearing stresses, and, also decreases the total volume and the material tends to acquire density close to the theoretical as reported elsewhere [16 - 20]. Densification in P/M preforms during deformation is thus reported to be dependent upon the mode of loading, preform geometry and its initial density, the pore shape, size and its distribution inside the preform [16-24]. However, during hydrostatic deformation, yielding and densification of P/M preforms take place as reported elsewhere [16, 17]. The material during upsetting mode laterally expands and when there is a restrain, which can develop hydrostatic pressure as well, and the same would create the feasibility of virtually attaining cent per cent density. The influence of shear mode of deformation has been described by Koerner [25]. The effect of strain induced densification and the stress-induced densification has been shown by Bockstigel and Olsen [18], Kuhn [4] and Fischmeister et.al [19]. However, the amount of flow or strain imparted to a preform is important in achieving high impact strength values [27]. Technical papers dealing on the deformation behaviour of sintered ferrous P/M preforms are described elsewhere [28 - 35] and for non-ferrous porous preforms can be referred in the recent literature [13, 36, 37]. The findings of these researchers have shown that the densification is a function of applied stress which induces strains and, therefore, relations have been proposed between the attained density and the true height strains. The present investigation is aimed to establish the feasibility of processing AISI 9840 steel prepared via the P/M route by exclusively using the elemental powders. Further, it is to develop the empirical relations for densification during hot forging of sintered P/M preforms. Also to study the influence of preform geometry on the densification mechanism. It is also planned to investigate bulging ratio and the densification, Poisson's ratio and densification modes. The AISI 9840 steel composition is Fe - 0.40 % C - 0.80% Mn - 0.30 % is - 0.80 % Cr - 1.0 % Ni - 0.25% Mo. Basically AISI 9840 steels come under the category of triple alloy steels, which include nickel, chromium and molybdenum. These steels exhibit high strength and strength to weight ratio apart from being good corrosion resistant. The presence of various alloying elements and their functions are discussed briefly here in section I.1.

## **I.1 Functions of Alloying Elements in AISI 9840 Steel**

### **1.1.1 Carbon**

Properties of iron-carbon alloys are greatly dependent upon the amount of carbon present in the steel. Once the carbon content is very low in the steel, the steel becomes very soft. However, an increase in the carbon content in the steel enhances its hardness and strength and ultimately the steel becomes very brittle once the carbon content into it exceeds 2.0 per cent. Basically, the carbon content has been taken as the basis for the characterization and classification of the iron-carbon alloys. They have been classified as the irons, steels and the cast irons. Thus, carbon is treated as an essential element in steel. Principally this element is added to increase the solid solution strength and hardness as well as to enhance the hardenability. It also dissolves in iron to form ferrite and austenite. It also combines with iron to form carbide called cementite ( $Fe_3C$ ) as a component of pearlite.

### **1.1.2 Nickel**

Nickel refines the grain size, improves hardenability and makes austenite to transform sluggishly. It further enhances the strength and toughness of ferrite. Combined with chromium it has a tendency to considerably improve the high temperature resistance to oxidation and corrosion. A nickel addition of 36 % in iron produces an alloy of almost zero expansion. Steels containing nickel in the range of 1.0 to 3.0 % are used for locomotive bodies, boilers, bolts, railway axles and large forgings. Higher amounts of nickel is added to increase the corrosion resistance of high chromium steels. Since it enhances the impact resistance of steel at very low temperatures, and, therefore, the same is extensively used in the manufacture of low temperature steels. Nickel steels were the first alloy steels that were used in large engineering applications such as armor plates, highly stressed bridge members, shafts etc. Further nickel induces improvement in mechanical properties after annealing and normalizing. Therefore, these steels are used for large forgings, castings and structural parts. Nickel is widely used in the production of stainless steels.

### **1.1.3 Manganese**

Manganese is present in all grades of steels and is used as a major deoxidizer. Elimination of hot shortness is one among the most important functions of manganese. It strengthens ferrite and is a mild carbide former. It further improves hardenability of steels and also makes austenite sluggish to transform. Apart from these, manganese is one among the least expensive alloying elements and is always present in almost all steels. It is an important alloying element in free cutting steels. This is also found invariably in all structural steels as well. Manganese, basically dissolves in ferrite and, thus, increasing its strength and hardness. Apart from these, it enhances the hardenability to a greater extent. It takes care of the harmful effects of sulphur by forming manganese sulphide. For this purpose the addition of manganese in steels are maintained at least three times that of the sulphur present in the steel.

### **1.1.4 Silicon**

Basically silicon dissolves in ferrite increasing its strength and hardness without lowering the ductility. Silicon hardens ferrite and enhances its hardenability moderately. It is a strong deoxidizer for steels and allows the production of sound steel. It is also a very strong graphitizer. Silicon and manganese put together impart high strengths to steels. Silicon-manganese structural and spring steels are the examples. Further, silicon is present in almost all grades of steels. Around 0.3 to 0.5 per cent silicon is added to steel castings in order to enhance their strengths and soundness. However, up to 5 per cent silicon is used in all magnetic steels such as in the steels used for the production of transformers, motors and generators. In these steels, silicon enhances the permeability of the steel and reduces iron losses. Thus, silicon is present in almost all the steels as it is an important alloying element in the steel. Silicon added in the spring steels, chisels and punches in order to enhance their toughness.

### **1.1.5 Chromium**

Chromium is less expensive alloying element in steels than nickel and it is capable of forming simple carbide (Cr<sub>3</sub>C), (Cr<sub>7</sub>C<sub>3</sub>) or complex carbides [(Fe Cr)<sub>3</sub>C]. These carbides have very high hardness and good wear resistance. Chromium is soluble up to 13% in  $\gamma$  - iron and has unlimited solubility in  $\alpha$ - ferrite. When chromium is present in amounts in excess of 5%, the steel is inherited with the high temperature properties and the corrosion resistance improvements. Chromium enhances the hardenability to such an extent that chromium steels are readily hardened even in very thick sections. Chromium forms carbides which are very hard and wear resistant. Further chromium imparts the steel the desired strength, wear resistance and oxidation resistance at elevated temperatures. Apart from these, chromium is a principal alloying element in all forms of stainless steels.

### **1.1.6 Molybdenum**

Molybdenum is relatively expensive alloying element and has limited solubility in  $\gamma$  and  $\alpha$ -iron and is a strong carbide former. Molybdenum has a strong effect on hardenability and like chromium increases the high temperature hardness and strength of steels. Steels containing molybdenum are less susceptible to temper brittleness compared to other alloy steels. Addition of molybdenum ranging in between 0.15 to 0.30 per cent to steels is done in order to enhance the effects of other alloying elements such as manganese, nickel and chromium. Further this acts as a grain growth inhibitor when the steel is subjected to elevated temperature applications. Molybdenum forms carbides having high red hardness and wear resistance. Further molybdenum resists softening of steel during tempering and heating cycles. Though, molybdenum is a relatively expensive alloying element and are generally found in almost all high strength structural steels. It is an important alloying element in high speed tool steels. Apart from these, molybdenum is commonly added to almost all carburizing steels.

## II. Experimental Details

### 2.1 Materials Required

The materials required to carry out the present investigation were powders of iron, graphite, manganese, silicon, nickel, chromium, and molybdenum respectively. The iron powder was procured from M/s. The Sundaram Fasteners Ltd., Hyderabad, Andhra Pradesh, India and the purity of iron powder was found to be 99.6% with 0.4% insoluble impurities. The main alloying powders such as Manganese, silicon, nickel, chromium and molybdenum powders of -37 urn were procured from M/s. The Ghrishma Enterprises, Mumbai, Maharashtra, India. The graphite powder of 2 - 5  $\mu\text{m}$  was supplied by The Asbury Graphite Mills, Inc., and Asbury Warren County, New Jersey, U.S.A., paste of graphite powder in acetone was used during powder compaction. Further, indigenously developed ceramic coating, electrically heated muffle furnace capable of maintaining  $1150^\circ \pm 10^\circ\text{C}$  temperature, ceramic rectangular boat for charging the indigenously developed ceramic coated preforms inside the furnace and suitable thermocouple for measuring the temperature were required. Apart from these, a hydraulic press of 1.0 MN capacity for powder blend compaction, and a friction screw press of 1.0 MN capacity for carrying out hot upset forgings were required. Suitable die, punch and the bottom insert assembly was required for powder compaction including the flat die set for hot upsetting experiments.

### 2.2 Powder Characterization

The basic properties such as the flow rates, apparent densities and compressibility tests were carried out for.

**Table I.** Characteristics of Iron Powder and AISI 9840 steel composition

SI. No.	Property	Iron	AISI 9840 Blend
1.	Flow rate by Hall Flowmeter, Sec/50g	23.80	25.00
2.	Apparent Density, g/cc	3.30	3.35
3.	Compressibility, g/cc at a pressure of 430 $\pm$ 10 MPa	6.64 $\pm$ 0.01	6.65 $\pm$ 0.01

Iron powder and the powder blend corresponding to AISI 9840 steel composition and the same are listed in Table I. However, the alloying elemental powders were taken to be of -37 $\mu\text{m}$  size, whereas, the sieve size analysis of the iron powder is tabulated in Table II.

**Table II.** Sieve Size Analysis of Atomized Iron Powder

Sieve Size, $\mu\text{m}$	-180+ 150	-150+125	-125+106	-106+90	-90+75	-75+63	-63+53	-53+45	-45+37	-37
Wt. % Ret.	3.61	3.62	2.48	0.70	8.33	9.20	16.68	15.83	3.59	35.90
Cum. Wt.%	3.61	7.23	9.71	10.41	18.74	27.94	44.62	60.45	64.04	99.94

### 2.3 Powder Blend Preparation

Elemental powders of iron, graphite, nickel, silicon, manganese, chromium and molybdenum in the required proportions were pre-weighed and mixed together and kept in a stainless steel pot with porcelain balls of 10mm to 15mm diameter and the pot lid was very securely tightened. The powder to ball ratio was maintained as 1.1: 1 by weight. Now, stainless steel pot was securely placed on the pot mill stand and tightened on it, and the machine was switched on. The blending operation was carried out for a period of thirty hours in order to obtain a homogeneous powder blend Once he uniformity in flow rates and apparent densities were obtained by carrying out an hourly tests on the powder mix, This test was carried out by stopping the pot mill after an interval of 1 hr. and taking out nearly. 100g powder blend for carrying out the flow rate and apparent density tests. Once the tests were completed, the powder blend was returned back to the steel pot. This test was carried out after an interval of every one hour of blending. Once the consistency in readings of flow rates and apparent densities were obtained the blending operation was terminated. Now the powder blend was ready to be used for further processing such as the preparation of the green compacts.

### 2.4 Compact Preparation

Compacts of 27.5mm diameter and 12 to 24mm heights were prepared from the powder blend of AISI 9840 steel composition in the density range of  $84.5 \pm 0.5$  per cent of theoretical by applying the pressure in the range of  $460 \pm 10$  MPa and by taking the pre-weighed powder blends. During the compact preparation, the inner die wall, the punch surfaces and the bottom insert surfaces were well lubricated by using graphite paste in acetoneso as to reduce the friction between the die walls and the powder particles and between the die wall and

the moving punch and also to facilitate easy ejection of the compacts at comparatively lower loads without damaging the compact surfaces, and, thus, minimizing the wear and tear of the die and punch surfaces. Compacts of three initial aspect ratios, namely, 0.45, 0.68 and 0.92 respectively were prepared on a 1.0 MN capacity Universal Testing Machine (UTM). Fig.1 shows the schematic diagram of complete powder compaction assembly. The same was used to prepare all the compacts each aspect ratio.

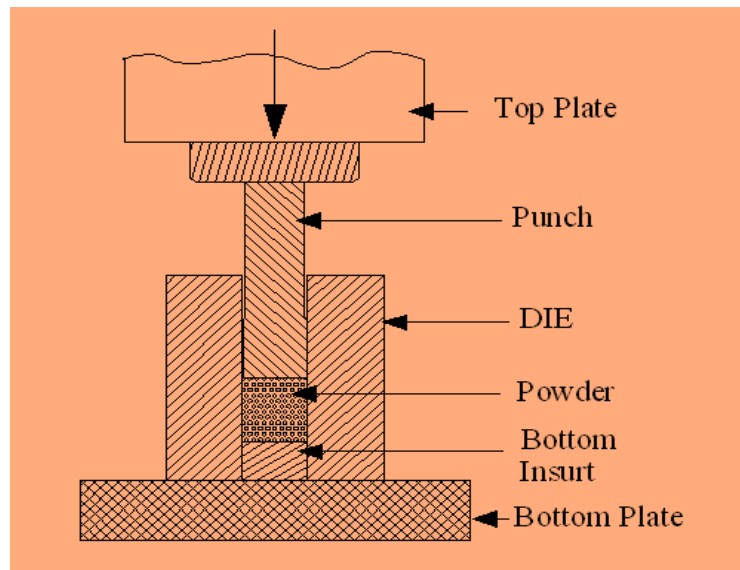


**Figure 1** Schematic Diagram of Showing the Complete Powder Compaction Assembly

### **2.5 Ceramic Coating, Drying, Sintering and Hot Axial Forging**

Compacts prepared from AISI 9840 powder blend were coated by indigenously developed ceramic coating [38] and this coating was allowed to dry under an ambient conditions for a period of 10-12 hrs. Immediately after the drying of the ceramic-coated compacts a second coating was applied 90° to the direction of the previous coating and the same was allowed to dry under the aforementioned conditions for a period of 12hrs. Ceramic-coated compacts of AISI 9840 powder blend were kept in a ceramic boat and charged into an electric muffle furnace in the uniform temperature zone for sintering at  $1150^0 \pm 10^0\text{C}$  for a period of 90 minutes. Once the ceramic-coated compacts were sintered they were immediately axially hot upset forged to varying strain levels. This exercise was carried out to all preforms of different aspect ratios, namely, 0.45, 0.68 and 0.92 respectively. Immediately after hot upset forging was carried out, the deformed preforms were quenched in oil kept at room temperature. Once the deformed preforms were taken out from the quenchant oil they were thoroughly cleaned. The residual ceramic coating was removed by gentle grinding/machining. The ground and the machined specimens were further smoothed by using emery papers and then they were ready for dimensional measurements and density evaluations. Dimensional measurements such as forged heights ( $H_f$ ), contact diameters {top ( $D_t$ ) and bottom ( $D_b$ )} and bulged diameters ( $D_b$ ) were made by using digital Vernier calipers. A minimum of three readings were taken and averaged out. Measurements were taken before and after removing the residual ceramic coatings. Virtually no substantial difference in dimensional measurements was found before and after the removal of ceramic coatings. However, the mass in air and water were found out by using single pan electronic balance [39] following the procedure described elsewhere [40].

## **II. Results and Discussion**

### **3.1 Deformation and Densification**

Fig. 2 has been drawn between the fractional theoretical density and the true height strain during the hot upset forming of sintered AISI 9840 P/M steel produced by using elemental powders. These plots also indicate the influence of initial preform aspect ratio, i.e., height to diameter ratio. A general observation of the curves in fig. 2 reveals that the characteristic nature of the curves are quite similar to each other. The preforms of smaller aspect ratio,

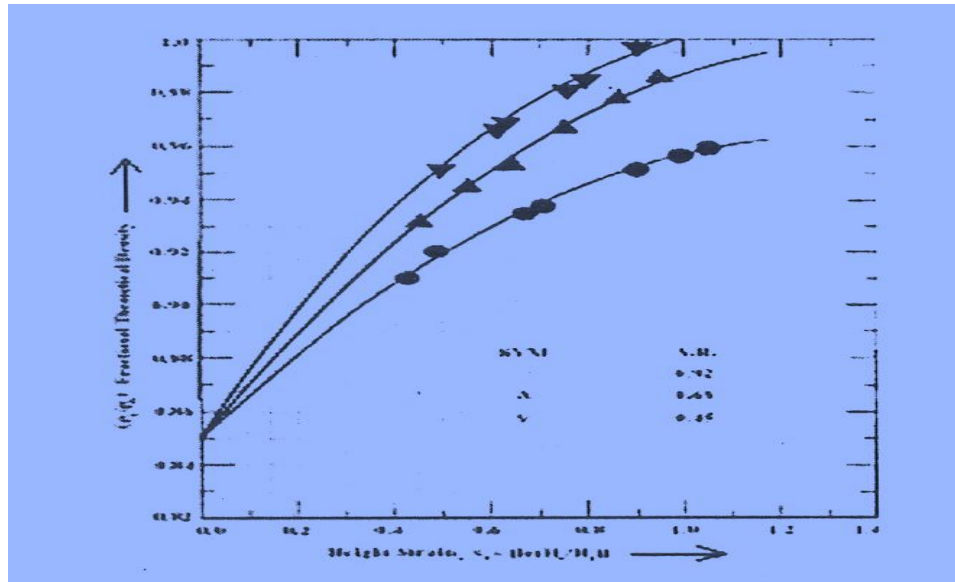


**Figure 2** Plots between the Fractional Theoretical Density ( $\rho_f/\rho_{th}$ ) and the True Height Strain ( $\epsilon_h$ ) During Hot Deformation of Sintered AISI 9840 P/M Steels of Different Initial Aspect Ratios.

i.e.,  $(H_0/D_0) = 0.45$  densified much more rapidly compared to the larger aspect ratio preforms, namely,  $(H_0/D_0)$  ratios of 0.68 and 0.92 respectively. Further analysis of these curves have revealed that the fractional theoretical density attained followed a third order polynomial with the variable called true height strain, i.e.,  $\epsilon = \ln(H_0/H_f)$ . The equation to which these curves corresponded very closely is mathematically expressed as:

$$(\rho_f/\rho_{th}) = a_0 + a_1\epsilon_h + a_2\epsilon_h^2 + a_3\epsilon_h^3 \text{----- (1)}$$

Where,  $(\rho_f/\rho_{th})$  is the fractional theoretical density and ‘ $a_0$ ’, ‘ $a_1$ ’, ‘ $a_2$ ’ and ‘ $a_3$ ’ are found to be empirically determined constants. The values of the constant ‘ $a_0$ ’ is found to be in close proximity to the initial preform density for each aspect ratio and, hence, it was concluded that this constant did not participate in the densification mechanism. Densification process in the first phase, is attributed to be linear as the constant ‘ $a_1$ ’ is linearly multiplied by the true height strain. Therefore, in the initial stages of the densification, the densification mechanism is absolutely linear. However, the value of the constant ‘ $a_2$ ’ is always found to be negative, and, therefore, the linearity of densification is disrupted and the curve - flattening step is introduced. Therefore, in the second stage of deformation, the densification starts retarding more and more if the initial aspect ratio has been kept increasing. It is also found that the values of constant ‘ $a_3$ ’ are either negative or positive depending upon the preform geometry. When it is found to be positive it has contributed to densification mildly and when the same was found to be negative it has retarded densification further more than what was observed to be only retarding in the second stage of densification. The values of these constants, i.e., ‘ $a_0$ ’, ‘ $a_1$ ’, ‘ $a_2$ ’ and ‘ $a_3$ ’ are listed in Table II along with the values of the regression coefficient  $R^2$ .

**Table III.** Coefficients of the Third order polynomial of the form:  $(\rho_f/\rho_{th}) = a_0 + a_1\epsilon_h + a_2\epsilon_h^2 + a_3\epsilon_h^3$  for AISI 9840 P/M Steel during Hot Deformation

Aspect Ratio	Constants				Regression Coefficient, $R^2$
	$a_0$	$a_1$	$a_2$	$a_3$	
0.45	0.85	0.284	-0.18	0.047	0.9997
0.68	0.85	0.219	-0.09	0.005	0.9999
0.92	0.85	0.164	-0.05	-0.01	0.9999

Table IV provides the level of densities achieved in preforms of three different aspect ratios, namely, 0.45, 0.68 and 0.92 respectively at the prefixed height strains. It is interesting to note that at every prefixed height strain, the densities achieved in lower aspect ratio preforms was higher than the next higher aspect ratio and further higher than the next largest aspect ratio preforms investigated in the present study. This also goes to confirm that the lower aspect ratio preforms densified much more rapidly compared to the larger aspect ratio preforms due to the quick and uniform load

**Table IV.** Fractional Theoretical Density Levels Achieved at Fixed Height Strains

Sl.No.	Fixed Strain	Aspect Ratio		
		0.45	0.68	0.92
1.	0.00	0.85	0.85	0.85
2.	0.10	0.876	0.870	0.865
3.	0.20	0.898	0.889	0.880
4.	0.30	0.919	0.907	0.895
5.	0.40	0.937	0.923	0.908
6.	0.50	0.952	0.938	0.918
7.	0.60	0.966	0.957	0.930
8.	0.70	0.978	0.963	0.937
9.	0.90	0.995	0.980	0.952
10.	1.0	0.999	0.987	0.957

transfer all across the preform thickness. The larger aspect ratio preforms densified poorly compared to the lower aspect ratio preforms due to more dampening behaviour as they contained more number of pores in the thickness direction. These results are in agreements with others [10, 29-34].

**3.2 Deformation, Densification, Strains and Concept of Poisson’s Ratio**

Basically, the Poisson's ratio ( $Y_p$ ) for porous materials under axial compression is defined as the ratio between the diametrical spread out,  $\epsilon_d = \{\ln (D_t/D_o)\}$  and the height strain, i.e.,  $\epsilon_h = \{\ln (H_o/H_t)\}$ , i.e.,  $Y_p = \epsilon_d/\epsilon_h$  which is a very sensitive parameter in metal forming operation when the deforming material is porous. In order to understand its actual significance, a plot between the diameter strain ( $\epsilon_d$ ) and the true height strain ( $\epsilon_h$ ) has been plotted in fig. 3 for all the

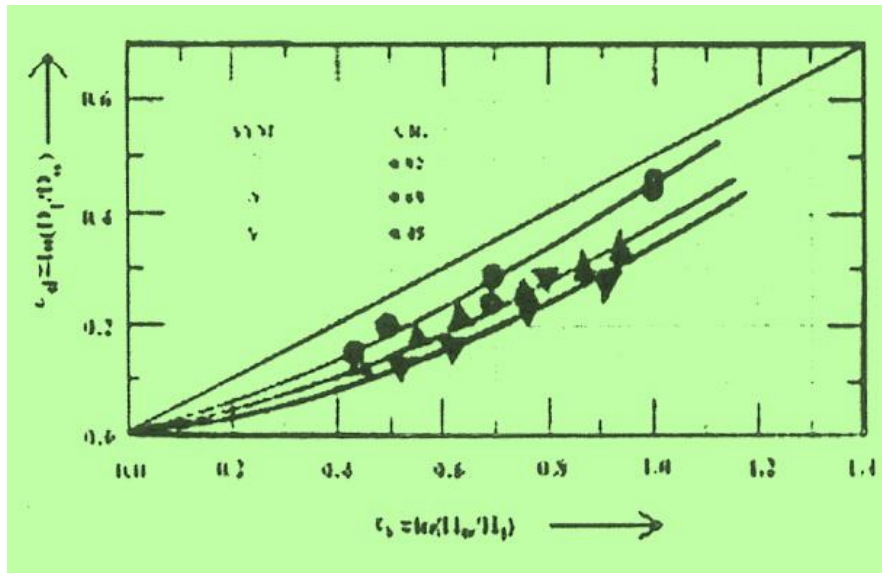


**Figure 3** Relationship between True Diameter Strains ( $\epsilon_d$ ) and the True Height Strains ( $\epsilon_h$ ) during Hot Axial Deformation of AISI 9840 Sintered Powder Preforms

aspect ratios during hot deformation of the sintered AISI 9840 P/M steel, It is observed that all the curves exhibit similar characteristic features, but, the curves corresponding to higher aspect ratio preforms are nearer to the theoretical line whereas the lower aspect ratios preform curves is the farthest away from the theoretical line. Interestingly all the data points are below the theoretical line which is the true representation of Poisson's ratio of the. Conventionally dense material under plastic deformation with virtually no friction, thus, yielding a slope of 0.5. Therefore, it can be confidently established that the Poisson's ratio ( $Y_p$ ) for porous materials under plastic deformation can never attain the limiting value of 0.5. Hence, it will always be a quest for the scientist to continue experimenting so as to acquire the value of the Poisson's ratio equal to 0.5 and also to attain the density very much close to one hundred per cent. This limiting value is not attained due to the fact that in the later stages of densification, the flow of pores and materials become simultaneous. This situation generally arises during axial upset forming operation and the same is reported elsewhere [29-37].

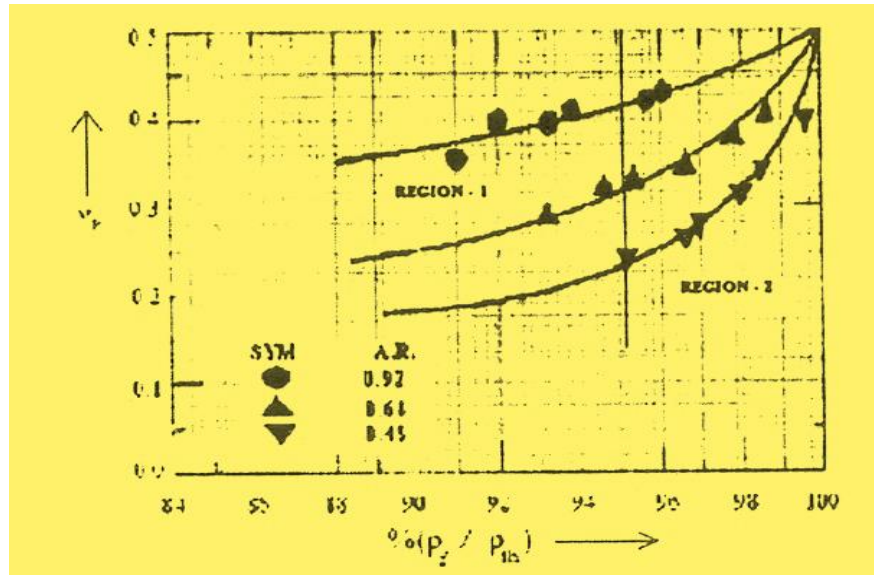


**Figure 4** Relationship between Poisson's ratio ( $Y_p$ ) and percentage theoretical density attained during hot axial deformation of AISI 9840 powder preforms

In order to establish the true behaviour of Poisson's Ratio with respect to the percentage density achieved, a plot between the Poisson's Ratio and the per cent theoretical density has been drawn and the same is shown in fig. 4. This fig. 4 very clearly shows the influence of initial preform geometries on the actual variation of Poisson's Ratio w.r.t. the attained per cent theoretical density during the hot axial upset forging of sintered AISI 9840 P/M steel preforms. The basic characteristic nature of all these curves are observed to be quite similar to each other, and therefore these curves can be mathematically expressed by a similar expression. A typical curve fitting analysis has revealed that they can be expressed by the following second order polynomial:

$$(p) = b_0 + b_1 (\rho_f/\rho_{th}) + b_2 (\rho_f/\rho_{th})^2 \text{----- (2)}$$

Where, 'b<sub>0</sub>', 'b<sub>1</sub>' and 'b<sub>2</sub>' are empirically determined constants and are found to depend upon the initial preform geometries of the system investigated. All these constants along with the values of the regression coefficients 'R<sup>2</sup>' are listed in Table V. Since, the values of the regression coefficient 'R<sup>2</sup>' in each case is found to be in extremely close proximity to unity, and, therefore the above empirical relationship arrived at is ably justified. Further, it is observed

**Table V** Coefficients of the Second order Polynomial of the Form:  $(p) = b_0 + b_1 (\rho_f/\rho_{th}) + b_2 (\rho_f/\rho_{th})^2$  for AISI 9840 P/M Steel during Hot Deformation

Aspect Ratio	Constants				Regression Coefficient R <sup>2</sup>
	b <sub>0</sub>	b <sub>1</sub>	b <sub>2</sub>	b <sub>3</sub>	
0.45	0.85	0.284	-0.18	0.047	0.9997
0.68	0.85	0.219	-0.09	0.005	0.9999
0.92	0.85	0.164	-0.05	-0.01	0.9999

From the above plot that the curves drawn in fig. 4 can be very explicitly sub-divided into two distinct two regions, namely, the Region-1 where densification occurred with a rapid pace, but, with a gradual increase in the values of the Poisson's Ratio and the Region-2 exhibited a rapid rise in the values of the Poisson's Ratio, but, with a minimal increase in attained density. This phenomenon has been true irrespective of the initial preform geometries. Thus, Region-1 is attributed as the region where maximum densification took place. However, Region 2 is described as a region where the pores that are left after the region-1, do not close down and their flow acquires the same status as that of the material flow. In other words, it can be established that the pores have technically stabilized in the structure just like a second phase and thus have become part and parcel of the structure itself. In this region, though the Poisson's ratio tends to approach to a limiting value of 0.5 in the near vicinity of the percentage theoretical density, but, it never attains the limiting value of 0.5. Therefore, it is imperative to conclude that the region 1 is the region of actual densification where the Poisson's ratio could rise steadily and the density enhancement becoming comprehensively rapid, and, hence, it is obvious to predict that in this region the pore closure kinetics is expectedly rapid while there is a gradual change in the geometry of the deforming preform, Now under the aforesaid arguments, it can be categorically stated that the region 2 is a zone

where pore closure kinetics for all practical purposes is a non - operative phenomenon, and, hence, the remaining pores left after region-1 become part and parcel of the structure itself.

### 3.3 Densification and the Bulging Ratio

In order to establish the relationship between the fractional theoretical density and the bulging ratio, fig.5 has been drawn between the parameters stated above. This figure demonstrates that the characteristic nature of these curves are quite similar to each other, but, the influence of geometry is found to be predominant. The curves of lower aspect ratio preforms are placed higher to the other aspect ratio curves. To further assess the influence of initial aspect ratio on the densification behaviour and bulging ratio, Table VI has been derived from fig. 5. This table shows that as the bulging ratio is kept constant, say for example 1.30, the density attained is 0.978, 0.947, and 0.916 in preforms of initial aspect ratios, i.e., 0.45, 0.68 and 0.92 respectively. This implies that the lower aspect ratio preforms have densified more rapidly compared to higher aspect ratio preforms. Further, as the bulging ratio is enhanced, the density in each aspect ratio has continued to increase. Further analysis of these curves in fig 5 has revealed that they have conformed to a second order polynomial of the form:  $(\rho_f/\rho_{th}) = b_0 + b_1 (D_b/D_0) + b_2 (D_b/D_0)^2$ ; where,  $(\rho_f/\rho_{th})$  is the fractional theoretical density and 'b<sub>0</sub>', 'b<sub>1</sub>', and 'b<sub>2</sub>' are empirically determined constants and they are found to depend upon the initial preform geometries. Further, the curves start to plateau, i.e., flattening in the final stages of deformation. Yet another mode of analyzing the relationship between the per cent theoretical density attained and the bulging ratio is to plot the curves between Log  $\{\rho_f/\rho_{th}\}$  and Log  $(D_b/D_0)$ . Such plots are shown in fig. 6. The data points on this plot for each aspect ratio exhibit a separate straight line indicating the fact that they actually represent a power law equation of the form:  $\rho_f/\rho_{th} = A (D_b/D_0)^m$  where 'A' and 'm' are found to be empirically determined.

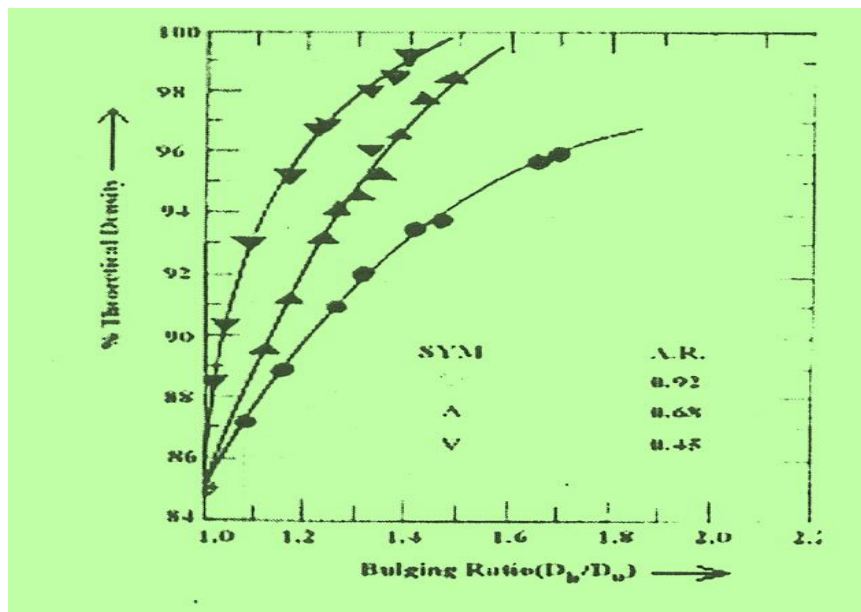
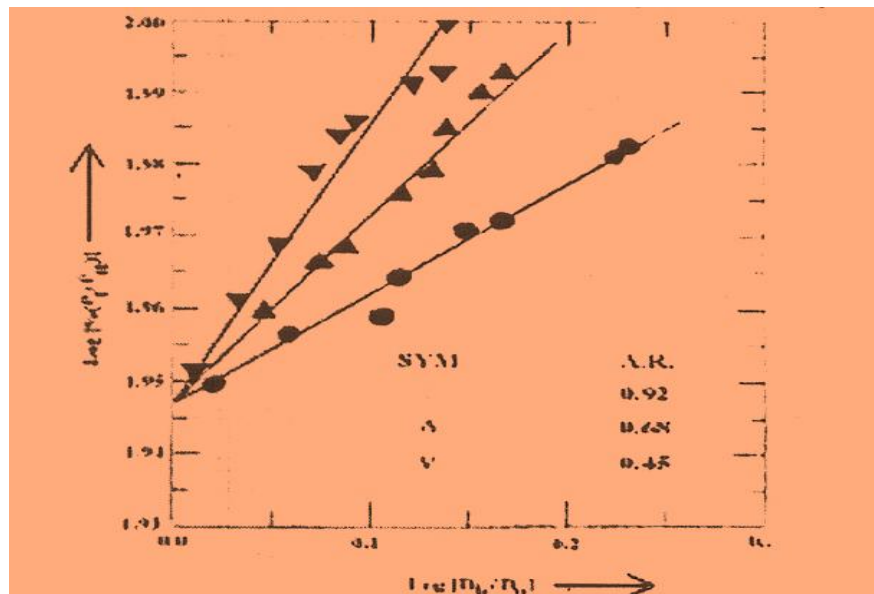


Figure 5 Relationship between Percentage Theoretical Density and Bulging Ratio during Hot Forging of AISI 9840 Powder Preforms.

Table VI. Level of Densification Achieved at Constant Bulging Ratio in the Preforms of Differing Aspect Ratio

S. No.	Bulging Ratio	A.R.=0.45	A.R.= 0.68	A. R.=0.92
1.	1.00	0.850	0.850	0.850
2.	1.05	0.905	0.870	0.863
3.	1.10	0.931	0.888	0.876
4.	1.20	0.961	0.921	0.889
5.	1.30	0.978	0.947	0.916
6.	1.35	0.988	0.960	0.924
7.	1.45	0.995	0.977	0.937
8.	1.50	---	0.984	0.943
9.	1.55	---	0.991	0.948
10.	1.60	---	---	0.953



**Figure 6:** Relationships between Log (Percentage Theoretical Density) and Log (Bulging Ratio) During Hot Forging of AISI 9840 Powder Preforms.

**Table VII.** Constants of the Power Law Equation of the form:  $\%(\rho_f/\rho_{th}) = A (D_b/D_o)^m$

Initial Aspect Ratio	Constants	
A. R.	'A'	'm'
0.45	88.51	0.384
0.68	88.51	0.256
0.92	88.51	0.152

constants and are further found to depend upon the initial aspect ratio of the preforms. The constant 'A' is found to be very close to initial preform density and therefore, is not responsible to contribute to densification whereas the value of 'm' is differing for each aspect ratio and, hence, it is attributed to contribute to densification. All of these constants are tabulated in Table V. Once the constants 'A' and 'm' have been determined, the accuracy of the main equation arrived at has been tested. Now for the fixed values of  $(D_b/D_o)$ , the corresponding values of the percentage theoretical

**Table VIII.** Measured and Calculated Values of  $\%(\rho_f/\rho_{th})$  and also the %age Error Observed

A.R.	$(D_b/D_o)$	$(\rho_f/\rho_{th})$ meas.	$(\rho_f/\rho_{th})$ cal.	%error
0.45	1.1	93.20	92.03	-1.26
0.45	1.2	96.05	95.15	-0.93
0.45	1.4	99.10	100.96	+1.88
0.68	1.2	92.20	92.96	+0.82
0.68	1.4	96.90	96.70	-0.21
0.68	1.5	98.40	98.42	+0.02
0.92	1.2	89.90	91.21	+1.46
0.92	1.5	94.30	94.36	+0.06
0.92	1.8	96.50	97.01	+0.53

density has been taken and also by using the power law equation stated earlier, the corresponding values of the percentage theoretical density have been calculated and the possible error has been assessed. It has been found that the percentage error was confined to the lower values than +1.88 and -1.26. The actual values are shown in Table VIII. In most of the cases the calculated and measured values were in the range of  $\pm 1.5\%$ . Thus, this demonstrates the accuracy of the above power law equation.

#### IV. Conclusions

Based on the critical analysis of the experimental and calculated data the following major conclusions can be drawn from the present investigation:

[1]. Densification curves followed a third order polynomial of the form:  $(\rho_f/\rho_{th}) = a_0 + a_1\epsilon_h + a_2\epsilon_h^2 + a_3\epsilon_h^3$ ; where,  $(\rho_f/\rho_{th})$  is the fractional theoretical density obtained at a given true height strain, i.e.,  $\epsilon_h = \ln(H_0/H_f)$  and 'a<sub>0</sub>', a<sub>1</sub>, a<sub>2</sub>, and 'a<sub>3</sub>' are found to be empirically determined constants. The constant 'a<sub>0</sub>' was found to be in very much close proximity to the initial preform density, and, therefore, it has not contributed to densification. However, the constant 'a<sub>1</sub>' is always positive and has linearly contributed to densification. Its values kept on decreasing as the aspect ratio was enhanced. The always-negative values of 'a<sub>2</sub>' have resulted in flattening the curves in the later stages of deformation. 'a<sub>3</sub>' is found to increase or decrease the densification rates as its values fluctuated between a very narrow range of negative to positive magnitudes,

[2]. Density levels achieved at any given true height strains were found to be maximum in lower aspect ratio preforms and minimum in the highest aspect ratio preforms. This phenomenon is attributed to the fact that the load transfer across the height direction has been quite uniform and quick in lower height to diameter ratio preforms. Further the poor densification in larger height to diameter ratio preforms is attributed to the cushioning effect of the total porosity content in terms of volume and thus the size effect (preform height) has played the significant role,

[3]. The variation of diameter strain with respect to the height strain has shown that all the data points were below the theoretical line indicating that there is no possibility of Poisson's ratio acquiring a limiting value of 0.5 while deforming porous preforms in the plastic range of deformation. The influence of the preform geometry has played a very distinct role in affecting the positions of the curves,

[4]. The variation of the Poisson's ratio w.r.t. the percentage theoretical density for each aspect ratio is found to be quite similar to each other but the curve corresponding to the larger aspect ratio preform is above all the curves corresponding to lower aspect ratio preforms. Further, the variation of Poisson's ratio is observed to be in such a manner that two clear and distinct regions can be classified. Region 1 is the actual stage of densification where the Poisson's ratio steadily rises and the density enhancement becomes comprehensively rapid and, therefore, it is established that in this region the pore closure kinetics is rapid and effective. However, in Region 2 pore closure kinetics for all practical purposes is non-operative and, therefore, it is established that the flow of material and pores that are left after region I remain in the deforming preforms as part and parcel of the structure itself, and, (Db/D<sub>0</sub>)

[5]. It has been established that the densification followed a second order polynomial with the bulging ratio (D<sub>b</sub>/D<sub>0</sub>) of the form:  $(\rho_f/\rho_{th}) = b_0 + b_1(D_b/D_0) + b_2(D_b/D_0)^2$ ; where, 'b<sub>0</sub>', 'b<sub>1</sub>' and 'b<sub>2</sub>' are found to be empirically determined constants. Measuring the bulging ratio and knowing the constants 'b<sub>0</sub>', 'b<sub>1</sub>' and 'b<sub>2</sub>' it is possible to predict the densities attained in the preforms without resorting to the tedious mode of measurements. Alternatively, a power law relationship has also been established which can predict the percentage theoretical density in ± 1 per cent range quite accurately. The power law equation is mathematically described as  $\% (\square/\square_{th}) = A(D_b/D_0)^m$  where the symbols have their usual meanings.

#### REFERENCES

- [1]. H. C. P. Carpenter and I.M. Robertson, "The Metallography of Some Ancient Egyptian Implements", JI. of Iron and Steel Institute, Vol.121, 1930, pp417 -448.
- [2]. P. Ulfgummeson, "Modern Atomizing Techniques", Powder Metallurgy, Vol.15, No.29, 1972, pp 67 -94.
- [3]. K. S. Pandey, "Powder Preform Forging", Proceedings of the National Seminar on Advances in Metal Forming, METFORM -2000, MIT Campus, Anna University, March 2000, pp 46-51.
- [4]. H. A. Kuhn and C. L. Downey, "How Flow and Fracture Affect Design of Preforms for Powder Forging", Int. JI. Of P/M&Powder/Tech., Vol.10, 1974, pp 59 -66.
- [5]. H. N. Tiwari and R. Saran, "Analysis of Iron Powder Preform Forging", Trans. of PMAI, Vol.12, 1985, pp 83 -86.
- [6]. H. M. Skelly, "Powder Preform Forgings Made from a Blended Iron Powder", Physical Metallurgy Research Laboratories, Report, MRPIPMPL - 78 -101, 1978, pp 1-15.
- [7]. M. I. Koczak and H. Chung, "The Effect of Elemental Alloying and Sintering Temperature on the Cold Forming of Powder Metallurgy Nickel Steels", Powder Metallurgy Int. Vol.7, No.3 1975, pp 71 -74.
- [8]. H. A. Kuhn and C. L. Downey, "P/M Preform Design for Hot Forging", Proceedings of APMI - ASM Congress, 1971, pp151 -162.
- [9]. H. A. Kuhn, "Deformation Processing of Sintered Powder Materials", Ed. By H. A. Kuhn & A. Lawley, Academic Press, N.Y., 1978, pp 99 - 119.
- [10]. K. S. Pandey, "Salient Characteristics of High Temperature Forging of Ferrous Powder Preforms", Key Engineering Materials, Vol.29 -31, Trans. Tech. Publication, 1989, pp, 465 -486.
- [11]. P. W. Lee, "Fracture in Cold Forming of Metals - A Criterion & Model", Ph.D. Dissertation, Drexel University, Philadelphia, 1972.
- [12]. P. W. Lee and H. A. Kuhn, "Cold Test in Workability", Testing Techniques, G. E. Dieter, Ed. ASM, 1984.
- [13]. S. K. Suh and H. A. Kuhn, "Three Fracture Modes and Their Prevention in Forming P/M Preforms", Mod. Dev. In

- P/M, Ed. By P. W. Taubenblatt and H. H. Hausner, Vol.9, 1977 MPIF Princeton, NJ, p- 407.
- [14]. T. S. Rao and K. S. Pandey, "Development of Theoretical Relations During Deformation of Disc and Ring Shaped Preforms", Trans. of PMAI, Vol.15, 1988, pp15-22.
- [15]. H. A. Kuhn and C. L. Downey, "Deformation Characteristics and Plasticity Theory of Sintered Materials", Int. Journal of P/M, Vol.7, No.1, 1971, pp 15 -26.
- [16]. F. Stassi and O. Alia, "Flow and Fracture of Materials according to New Limiting Condition of Yielding", Vol.3, No.11, 1967, pp 28 -37.
- [17]. K. J. Kahlow, "Void Behaviour as Influenced by Pressure and Plastic Deformation", Institute of Metal Forming Report, Lehigh University, October 1971.
- [18]. S. M. Doraivelu, H. L. Gegel, J. S. Gunasekaran, J. C. Malas and J. T. Morgan, "A New Yield Function for Compressible PIM Materials", Int. J. Of Mech. Sci. Vol.26, No.9 -12, 1984, pp 527 -535.
- [19]. H. F. Fishmeister, B. Aren and K. E. Easterling, "Deformation and Densification of Porous Preforms in Hot Forging", Powder Metallurgy, Vol.14, No.27, 1971, pp 144 -163.
- [20]. H. W. Ante, "Deformation of Porous Materials", A - Report, Hoeganaes Corporation, Riverton, NJ, 1974, pp 1-
- [21]. R. Narayanasamy and K. S. Pandey, "Salient Features in the Cold Upset Forming of Sintered Aluminium - 3.5% Alumina Powder Composite Preforms", JI. of Mat. Proc. Tech., Vol.72, 1997, pp 201 - 207.
- [22]. R. Narayanasamy and K. S. Pandey, "Some Aspects of Work Hardening in Sintered Aluminium and Aluminium-Iron Composite Preforms During Cold Axial Deformation", JI. of Mat. Proc. Tech., Vol.84, 1998, pp 136 - 142.
- [23]. J. R. Inigoraj, R. Narayanasamy and K. S. Pandey, "Strain Hardening Behaviour in Sintered Aluminium - 3.5% Alumina Composite Preforms During Cold Axial Compression with or Without Annealing", JI. of Mal. Proc. Tech., Vol. 84, 1998., pp 143 - 148.
- [24]. A J. R Inigoraj, R. Narayanasamy and K. S. Pandey, "Densification in Aluminium and Aluminium-Alumina Sintered Preforms During Cold Deformation", JI. of Metals, Materials and Processing, Vol. 10, 1998, pp.167- 176.
- [25]. R. M. Koerner, "Tri-axial Compaction of Metal Powders", Powder Metallurgy International, Vol.3, No.4, 1971, pp.186-188.
- [26]. G. Bockstiegel and H. Olsen, "Processing Parameters in the Hot Forming of Powder Preforms", Third European Powder Metallurgy Supplement, Part-I, Powder Metallurgy (U.K.), 1971, pp.127-148.
- [27]. K. H. Moyer, "The Effect of Density on the Impact Properties of Iron PIM Forgings", Metals Engineering Quart., August 1972, pp.34-38.
- [28]. K. S. Pandey, P. S. Misra and M. L. Mehta, "Effect of Forging Temperature and Carbon Content on the Cracking Behaviour of Iron- Powder Preforms Hot Upset Forged", Trans. of P.M.A.I., Vol.15, 1988, pp.9-14.
- [29]. M. N. Rao and K. S. Pandey, "Working of Porous Solid Cylinders of Eutectoid Composition", 14th National AIMTDR Conference Proc.1990, pp.217-222.
- [30]. J. ArivudaiNambi and K. S. Pandey, "Densification Behaviour of Iron and AISI 4340 Powder Preforms During Hot Upsetting", Engineering Today, Vol.1, No.11, Nov.1999, pp.2-4.
- [31]. J. ArivudaiNambi and K.S. Pandey, "Assessment of Mechanical Properties of Hot Forged AISI 4340 PIM Steel", Engineering Today, Vol., No.12, Dec.1999, pp.19-21.
- [32]. S. Senthil Kumar, K. S. Pandey and P. Aravindan, "Densification Mechanism Operative During Hot Forging of Sintered AISI 4140 Steel Composition Using Elemental Powders", National Conference Proceeding on Quality Control in Metallurgical Industries, PSG College of Technology, Coimbatore - 641 004, Conf. Proc. 1999, pp. 76-83.
- [33]. N. Ponnusamy, K. S. Pandey and P. Aravindan, "Effect of Manganese Addition in Sintered Fe-1.0%C Hyper Eutectoid Steel During Hot Forging", *ibid*, pp.496-503.
- [34]. K. S. Pandey, "Powder Preform Forging", Proc. of the National Seminar on the Advances in Metal Forming, METFORM - 2000 held at M.L.T. Campus, Anna University, March 2000, pp.46-51.
- [35]. J. Anusha, J. ArivudaiNambi, K. S. Pandey and P. Aravindan, "Effect of Alteration of Chromium Percentage in AISI 4340 PIM Steel and Assessment of Mechanical Properties", *ibid*, pp.63-68.
- [36]. S. Ram Kumar, R. Narayanasamy, K. S. Pandey and K. Mathrubootham, "Effect of Residual Porosity on the Mechanical Properties of Cold Deformed Aluminium and Aluminium - 4% Cu Alloy Powder Preforms", Trans. of P.M.A.I., Vol., 15, 1988, pp.3-8.
- [37]. K. S. Pandey, "Some Investigation on the Cold Deformation Behaviour of Sintered AI-4%Cu Alloy Powder Preforms", Quart. Int. JI. of PIM Sci. &Tech., Yoi.2, No.3, 1991, pp.35-42.
- [38]. K.S. Pandey, "Special High Temperature Ceramic Coating Indigenously Developed to Protect Preforms Against Oxidation During Sintering", Regional Engineering College, Tiruchirappalli - 620 015, T.N., India, 1986.
- [39]. "Instructions Manual for Electronic Balances", Model-180, Adair Dutt & Co (India) Pvt. Limited, Madras.
- [40]. Siddhartha Pandey, R. Chandramouli, K. S. Pandey and P. Aravindan, "Densification Behaviour and Properties of Sintered Hot Forged Iron - Carbon - Titanium Carbide particles composites", Proc. Of National Conference on Recent Trends in Manufacturing Technology and Management, Adhiyamaan College of Engineering, Hosur - 635 109, Conf. Proc. 28-29 January 2002, pp.134-141.